Modes of three-dimensional dust crystals in dusty plasmas

Yuriy Ivanov and André Melzer
Institut für Physik, Ernst-Moritz-Arndt-Universität Greifswald, 17489 Greifswald, Germany
(Received 17 October 2008; revised manuscript received 7 January 2009; published 11 March 2009)

Three-dimensional finite systems of charged dust particles confined to concentric spherical shells in a dusty plasma, so-called "Yukawa balls," have been studied experimentally with respect to their dynamic properties. For that purpose, the three-dimensional thermal Brownian motion of the dust particles around their equilibrium positions was reconstructed with high accuracy. From that the dynamic properties in the form of mode patterns and frequencies are obtained from singular value decomposition and normal mode analysis. The dynamics of the Yukawa balls was found to be dominated by large-scale low-frequency shearlike modes.

DOI: 10.1103/PhysRevE.79.036402 PACS number(s): 52.27.Lw, 52.27.Gr, 82.70.Dd

I. INTRODUCTION

Finite clusters of particles are of enormous interest in physics and chemistry. On the nanometer scale, a vast number of atomic or molecular clusters with various types of interaction exist [1]. In dusty plasmas, Coulomb clusters with a finite number of micron-sized "dust" particles can be trapped in a gaseous plasma environment. There, the microparticles interact by a (screened) Coulomb repulsion at interparticle distances much larger than the particle size [2–6]. These finite dust clusters can serve not only as models for nanometric systems, but also allow deep insight into the behavior of strongly coupled plasmas in general.

Finite clusters are particularly interesting since many of their thermodynamic properties (e.g., melting temperature, latent heat or entropy change) dramatically depend on the exact number N of particles in the cluster [7]. Similarly, also the dynamics of a cluster decisively changes with N. Here, dusty plasmas provide an ideal tool to study cluster dynamics since the cluster motion can be measured by video microscopy on the kinetic level of individual particles. Dust clusters are highly transparent and their motion is only weakly damped.

Two-dimensional (2D) finite clusters in dusty plasmas have been widely studied experimentally in view of their structure and their dynamics [2,3,8–10]. As expected from simulations [11–13] the clusters form concentric rings with configurations that decisively depend on the particle number N. The dynamics of such 2D clusters has been studied from normal mode analysis and singular value decomposition (SVD) derived from the thermal Brownian motion of the dust particles around their equilibrium positions [3,10]. However, finite-size effects die out relatively quickly in 2D systems since already for particle numbers $N>50$, the 2D clusters show in the cluster center the hexagonal bulk order expected for infinite systems.

Three-dimensional (3D) clusters are expected to show finite-size effects to much higher particle numbers $N>10\,000$ [14]. It has now become possible to trap such spherical 3D clusters of charged microspheres in a plasma, where they form so-called "Yukawa balls" [4,5]. The microparticles arrange in nested, concentric spherical "onion" shells. The configurations are labeled $(N_1,N_2,\ldots)$ where N_1 is the number of particles in the inner shell, N_2 that of the next shell, etc. Such Yukawa balls have already been investigated experimentally in view of their structure [4,6,15] and slow transitions of particles between shells [16]. Also plasma-induced changes of particle number in the clusters have been observed [17]. However, a reliable analysis of the mode dynamics of Yukawa balls has not been possible so far.

Here, we present experiments on the mode dynamics of Yukawa balls. There, the 3D Brownian motion of the particle in the cluster was recorded and determined with sufficient accuracy to warrant the analysis of the modes. These modes have been derived from normal mode analysis and singular value decomposition which yield complementary information on the cluster dynamics.

II. EXPERIMENT AND DATA ANALYSIS

The experiments have been performed in an asymmetric capacitively coupled radio frequency discharge operated in argon at 13.56 MHz, a gas pressure of 90 Pa, and a discharge power of 7.5 W. The experimental setup is analogous to the one used in [4]. Monodisperse melamine formaldehyde spheres of 3.47 μm diameter have been dropped into the plasma to form 3D Yukawa balls. The scheme of the experimental setup and the confinement of a Yukawa ball are presented in Fig. 1. A square glass cuvette is placed onto the lower electrode for lateral confinement of the dust cloud. Vertically, the gravitational force on the particles is (partially) compensated by an upward thermophoretic force due to heating of the lower electrode. Additional levitation is provided by the sheath electric field above the lower electrode. These forces provide an isotropic 3D harmonic confinement potential in which the particles are trapped [18]. There, the particles arrange in the concentric spherical shells of the Yukawa ball. The dust particles are illuminated by an expanded laser beam at 532 nm. Three synchronized cameras record the particle motion from three orthogonal directions at a frame rate of 20 frames per second [16].

The reconstruction of the 3D particle positions makes use of the orthogonality of the cameras, since each pair of cameras shares one common coordinate axis. From this, corresponding particles and their positions can be uniquely identified in the different cameras. Thus, the 3D positions of the particles through all camera frames have been reconstructed. Even with overlapping images in one camera the position of

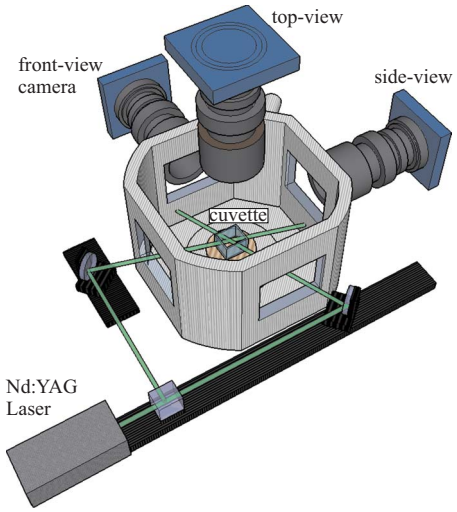

FIG. 1. (Color online) Scheme of the experimental setup.

the particles can be determined from the other two cameras [16]. For the experimental results presented here, special attention has been paid that all particle positions through all camera frames have been reconstructed. In some cases, visual inspection of the camera frames was necessary. Each particle then has been tracked through the entire sequence. Thus, we were able to determine the motion of several complete clusters through more than $F=1000$ frames each. Here, we focus on a cluster with $N=31$ and $F=1300$ frames. The mean reconstruction error was typically about 2 pixels whereas the mean Brownian particle excursions from the equilibrium were about 30 pixels. Thus, it was possible to extract the dynamics of the Yukawa balls from such video sequences. In the analysis of the dynamics two complementary techniques, the normal mode analysis and the singular value decomposition, have been applied.

To determine the normal modes, Yukawa balls are described by their potential and electrostatic energy

$$E = \frac{1}{2} m \omega_0^2 \sum_{i=1}^{N} r_i^2 + \frac{Z^2 e^2}{4\pi\epsilon_0} \sum_{i<j}^{N} \frac{\exp(-r_{ij}/\lambda_D)}{r_{ij}}, \tag{1}$$

where Z and m are the dust particle charge number and mass, respectively, $r_i=|\vec{r}_i|$ is the distance of the ith particle to the center of the confinement, and $r_{ij}=|\vec{r}_i-\vec{r}_j|$ is the relative distance between the particles i and j. The first term in Eq. (1) is the energy of the 3D isotropic parabolic confinement (with resonance frequency ω_0). The second term denotes the screened electrostatic interaction energy between the particles (with screening length λ_D). The corresponding screening strength $\kappa=b/\lambda_D$ is given as the ratio of the interparticle distance b in units of the screening length.

Then, the normal modes are the eigenvalues and eigenvectors of the dynamical matrix [12]

$$A_{\alpha,\beta,ij} = \frac{\partial^2 E}{\partial r_{\alpha,i} \partial r_{\beta,j}}, \tag{2}$$

where $r_{\alpha,i}$ denotes the x, y or z coordinate of the ith particle. There, we assume that the average positions of the N particles describe their equilibrium positions. The eigenvalues and vectors are then computed using the LAPACK routines of MATLAB [19].

Experimentally, the normal mode spectra are obtained as the spectral power density $S_\ell(\omega)$ from the Fourier transform for the mode number $\ell=1,\ldots,3N$ by

$$S_\ell(\omega) = \frac{2}{T} \left| \int_0^T v_\ell(t) e^{i\omega t} \right|^2. \tag{3}$$

Here, $v_\ell(t)=\Sigma_{i=1}^{N} \vec{v}_i(t) \cdot \vec{e}_{i,\ell}$ are the projections of the Brownian particle fluctuations with velocities $\vec{v}_i$ around their equilibrium positions onto the normal mode oscillation patterns $\vec{e}_{i,\ell}$ of the mode ℓ (see e.g. Ref. [3]).

The effective thermal energy of the modes of the Yukawa ball can be extracted from the normal mode spectra using the relation

$$\int_0^\infty S_\ell(\omega) d\omega = \langle v_\ell^2 \rangle \tag{4}$$

that yields the mean-square particle velocity of mode number ℓ from the power spectrum. The mode temperature is then simply related to the kinetic energy of the particles via

$$\tfrac{1}{2} k T_\ell = \tfrac{1}{2} m \langle v_\ell^2 \rangle. \tag{5}$$

Consequently, we can assign the effective temperature T_ℓ to each of the modes.

The method of singular value decomposition (SVD) makes use only of the particle trajectories without the necessity of assigning physical properties, such as the energy, to the system. There, first the data matrix

$$\mathbf{D} = \begin{pmatrix} x_1(1) & \cdots & x_1(F) \\ \vdots & \ddots & \vdots \\ x_N(1) & \cdots & x_N(F) \\ y_1(1) & \cdots & y_1(F) \\ \vdots & \ddots & \vdots \\ y_N(1) & \cdots & y_N(F) \\ z_1(1) & \cdots & z_1(F) \\ \vdots & \ddots & \vdots \\ z_N(1) & \cdots & z_N(F) \end{pmatrix} \tag{6}$$

is created from the experimental values of the particle positions. There $x_i(f), y_i(f), z_i(f)$ are the x, y or z coordinate of the ith particle in frame number $f=1,\ldots,F$. Then the data matrix that contains the full information of the particle trajectories is decomposed into three matrices as

$$\mathbf{D} = \mathbf{U} \mathbf{\Sigma} \mathbf{V}^T, \tag{7}$$

where $\mathbf{U}$ (*topos*) is a $3N \times 3N$ matrix containing the $3N$ SVD mode patterns in pairwise orthonormal columns [20]. Further, $\mathbf{V}$ (*chronos*) is a $F \times F$ orthonormal matrix that describes the temporal evolution of the modes. Finally, $\mathbf{\Sigma}$ is a $3N \times F$ diagonal matrix that contains the singular values $\sigma_\ell = \Sigma_{\ell\ell}$ describing the strength of the mode ℓ. The computation is again done using the LAPACK routines of MATLAB [19].

With SVD, the complete trajectory of all particles is decomposed into orthogonal mode patterns (contained in **U**) and their temporal evolution (contained in **V**). The relative contribution of mode ℓ to the total particle trajectories is given by the relative signal energy of mode ℓ as

$$p_\ell = \frac{\sigma_\ell^2}{\sum_{\ell'=0}^{3N} \sigma_{\ell'}^2}.$$

It should be noted that the signal energy does not define a physical energy stored in the mode since no physical description of the system enters the SVD analysis.

The SVD yields complementary information compared to the normal mode analysis (see, e.g., Refs. [10,21]) since SVD makes use only of the particle trajectories. The trajectory $\vec{r}_j$ of particle j at frame f can be reconstructed via

$$\vec{r}_j(f) = \sum_{\ell=1} \sigma_\ell U_{j\ell} V_{f\ell}^T$$

using the motion pattern $U_{j\ell}$ of mode ℓ, its time information $V_{f\ell}^T$ and the weight σ_ℓ. Since usually the weight σ_ℓ rapidly decreases with mode number, SVD identifies those mode patterns (and their temporal evolution) that make up the main features of the observed trajectories. Often only the first few modes contain most of the characteristics of the trajectories.

Hence, SVD identifies the dominant contributions to the motion of the particles by purely judging the trajectory. In contrast, normal modes yield information on the system from the harmonic expansion of the energy around the equilibrium positions. SVD is able to detect motion patterns that are not necessarily normal modes, possibly giving hints to unexpected behavior. Normal modes in turn allow us to extract the physical features according to the involved physical model.

III. EXPERIMENTAL RESULTS

The dynamic properties of different Yukawa balls have been determined from the recorded and reconstructed thermal motion using both normal mode analysis and SVD. Here, we concentrate on a Yukawa ball with $N=31$ particles. The dynamical properties of the other Yukawa ball support the findings for the $N=31$ cluster. We start the experimental analysis with a brief description of the structure of this specific Yukawa ball.

A. Structure of the Yukawa ball

The structure of the Yukawa ball is shown in Fig. 2. The dust cluster consists of $N=31$ particles that are arranged on two concentric shells with five particles on the inner and 26 particles on the outer shell. In Fig. 2(a) the particle trajectories over the entire sequence (1300 frames or 65 seconds) are shown. Here, cylindrical coordinates $\rho=(x^2+y^2)^{1/2}$ and z are used. It is seen that the particles only show a thermal Brownian motion around their equilibrium positions. The particles stay near their equilibrium positions throughout the entire sequence. From these thermal fluctuations the SVD and normal modes are extracted.

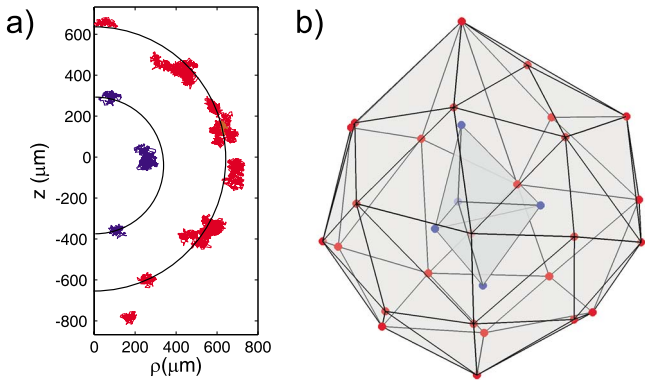

FIG. 2. (Color online) (a) Trajectories of the particles of the Yukawa ball with $N=31$ particles. The trajectories are shown over 1300 frames (65 seconds) in cylindrical coordinates. (b) Bond model of the dust cluster. The Yukawa ball forms two concentric shells with five particles on the inner and 26 particles on the outer shell.

For illustration, Fig. 2(b) also shows a bond structure model of the Yukawa ball for a single instant. The observed configuration (5,26) does not change during the sequence. It should be noted, however, that the configuration (5,26) is not the ground-state configuration. The ground state is (4,27) for a system of charged particles in an isotropic confinement according to Eq. (1) for experimentally accessible values of the screening strength $\kappa<2$ [22]. In contrast, (5,26) has been identified as a metastable configuration that is very frequently observed in experiments on Yukawa balls [15,16]. This, however, does not influence the identification of its dynamical properties.

B. SVD analysis

From the thermal Brownian motion of the dust particle in the Yukawa ball now the dynamical properties are addressed by the SVD analysis tools according to Eqs. (6) and (7). The 93 SVD modes have been calculated according to the above-mentioned procedure.

To gain a first overview over the various modes, the shear and compressional properties of the modes are calculated. Following Schweigert *et al.* [12] the shear and the compressional contribution of a mode are derived from the rotor and divergence of its eigenvector field as

$$\Psi_r^2(\ell) = \frac{1}{N}\sum_{i=1}^{N} \psi_{r,i}^2(\ell), \tag{8}$$

$$\Psi_d^2(\ell) = \frac{1}{N}\sum_{i=1}^{N} \psi_{d,i}^2(\ell), \tag{9}$$

where

$$\psi_{r,i}(\ell) = \frac{1}{M}\sum_{m=1}^{M} |(\vec{r}_i - \vec{r}_m) \times (\vec{e}_{i,\ell} - \vec{e}_{m,\ell})|/|\vec{r}_i - \vec{r}_m|^2,$$

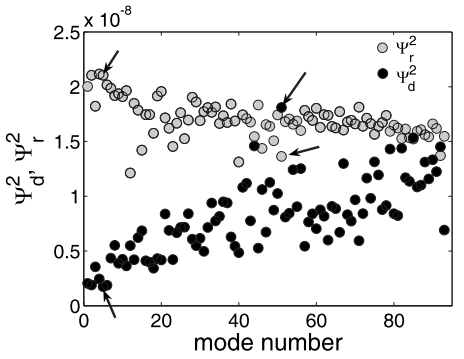

FIG. 3. Shear (Ψ_r^2) and compressional (Ψ_d^2) contribution of the 93 SVD modes of the $N=31$ Yukawa ball. For mode Nos. 5 and 51 the shear and compressional contribution are marked by an arrow. See text for details.

$$\psi_{d,i}(\ell) = \frac{1}{M}\sum_{m=1}^{M} (\vec{r}_i - \vec{r}_m)\cdot(\vec{e}_{i,\ell} - \vec{e}_{m,\ell})/|\vec{r}_i - \vec{r}_m|^2.$$

Here, m, M denote the index and number of neighboring particles to particle i (the neighbors of particle i are those within a range of 1.5 times the mean interparticle distance). Since the eigenvectors describe the direction and strength of the particle motion $\Psi_{d,r}^2(\ell)$ can be interpreted as analog of the divergence and rotor of the velocity field in extended systems. Thus, the averaged local divergence $\Psi_d^2(\ell)$ is the magnitude of the compressional contribution to mode ℓ, and the averaged local rotor $\Psi_r^2(\ell)$ gives its shear part.

Figure 3 shows the calculated shear and compressional contribution for all SVD modes. The mode numbers are sorted with respect to their relative signal energy (mode number 1 has the highest signal energy, mode number 93 the lowest, see Fig. 4). It is seen that generally the shear contribution $\Psi_r^2(\ell)$ is high for the first modes and slowly drops towards the higher modes. In contrast, the compressional contribution $\Psi_d^2(\ell)$ increases with mode number. Combining this with the relative signal energy this means that the most dominant modes are modes with high shear contribution, i.e., the dynamics is dominated essentially by shear modes.

We now like to discuss two modes more closely, namely mode Nos. 5 and 51. These modes contribute to the signal

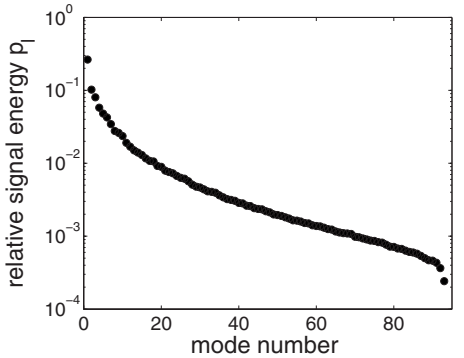

FIG. 4. Relative signal energy of the 93 SVD modes of the $N=31$ Yukawa ball.

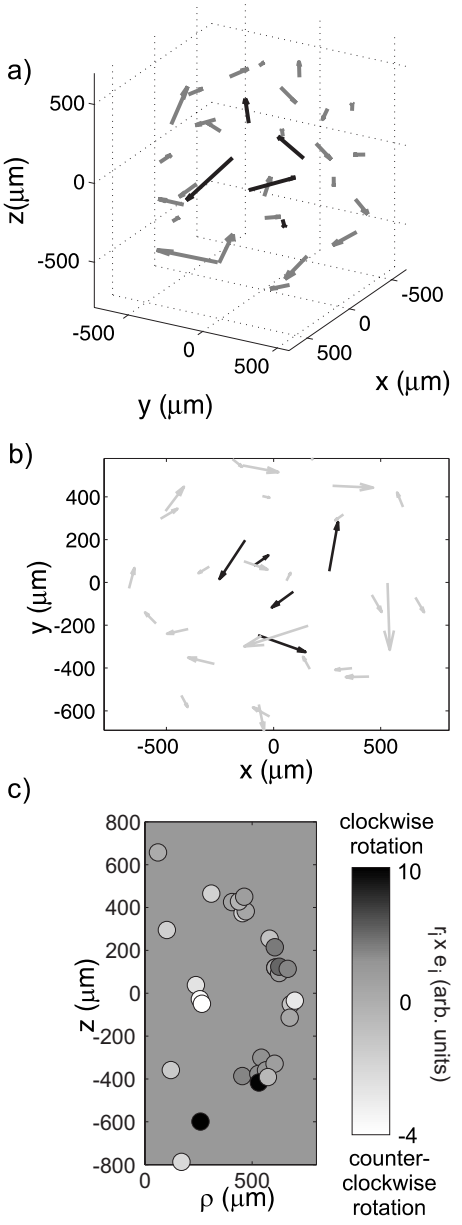

FIG. 5. (a) 3D mode pattern of the intershell rotation mode (mode No. 5). Black arrow indicates the motion of the particles on the inner shell, gray that of the outer shell. (b) Projection of the 3D mode pattern on the x-y plane. (c) Magnitude of shell rotation vectors in gray scale. The gray level of the figure background refers to zero rotation, hence lighter particles have counterclockwise rotation, darker particles rotate clockwise.

energy with 4.8% and 0.2%, respectively. Mode No. 5 is the mode with the highest ratio of Ψ_r^2/Ψ_d^2 and mode No. 51 that with the lowest ratio of Ψ_r^2/Ψ_d^2 (and also the one with the highest absolute value of Ψ_d^2). The mode pattern of these two modes is shown in Figs. 5(a) and 6(a).

Mode No. 5 closely resembles an intershell rotation mode where the inner and the outer shell rotate with respect to each other. This is already visible in the mode pattern. To illustrate that in more detail the rotary contribution of each particle $\vec{r}_i \times \vec{e}_i$ in this mode is calculated and is shown in gray scale in Fig. 5(b). Counterclockwise rotary contributions are shown

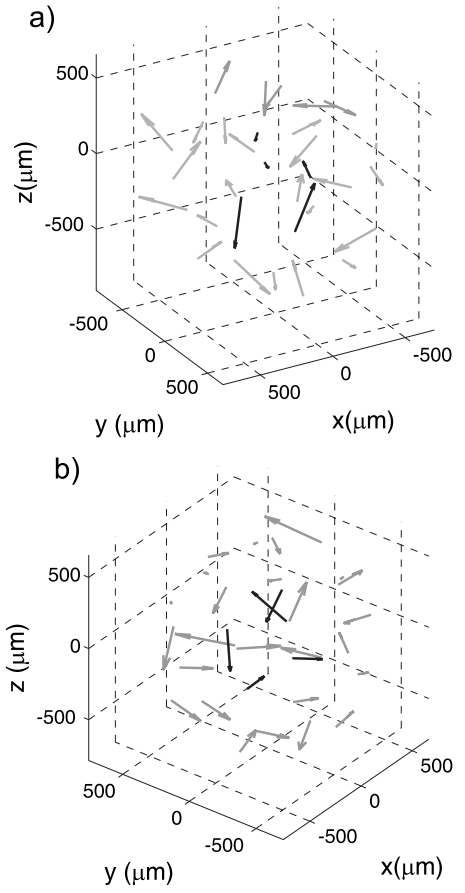

FIG. 6. (a) 3D mode pattern of the most compressional mode (mode No. 51) and (b) the mode with highest signal energy (mode No. 1).

in light gray, clockwise rotary contributions in dark gray. It is seen that the inner particles predominantly show a counterclockwise rotation whereas the outer shell predominantly rotates clockwise. This clearly demonstrates the intershell rotation mechanism. From all 93 modes, this mode No. 5 has the highest contribution to intershell rotation.

The most compressional mode No. 51 does not allow such a clear interpretation. However, it can easily be noted that the mode shows strong opposite motion between neighboring particles, especially between particles of the inner and outer shell, e.g., in the lower left or the central right region of Fig. 6(a). This opposite motion is a direct sign of the compressional character of this mode. The fact that the opposite motion is very local, among nearest neighbors, makes this mode the one with the highest compressional contribution.

The modes with the highest signal energy (modes No. 1 through No. 4), that account for about half of the total signal energy, describe rotations of the entire Yukawa ball around different axes or large-scale vortexlike motions. For illustration, the mode with the highest signal energy (mode No. 1) is shown in Fig. 6(b). The character of a global rotation can be very well deduced.

C. Normal mode analysis

Now, in a similar manner, the normal modes of the Yukawa ball with $N=31$ particles have been determined from the thermal Brownian motion according to Eqs. (1)–(3). Further, the spectral power densities of the modes have been calculated according to the procedure described in Sec. II.

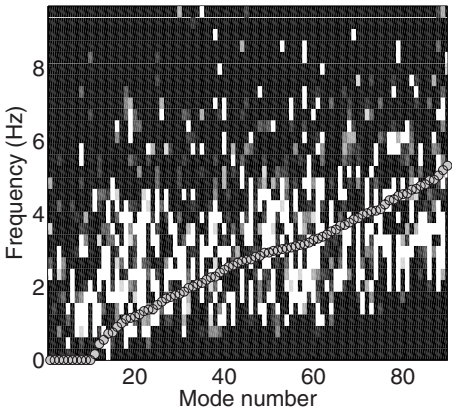

FIG. 7. Spectral power density (gray scale) as a function of frequency for the modes of the Yukawa ball. The calculated spectral power density increases from black to white. The gray circles are a best fit of the calculated eigenfrequencies to the spectral power density.

The spectral power density is shown in Fig. 7 for all modes of the Yukawa ball. There the modes have been ordered with increasing frequency. First, it is seen that we were indeed able to derive a reliable spectrogram. This is due to the fact that the mean reconstruction error was smaller than the mean displacement from the thermal motion. However, the spectral power density appears to be much broader in frequency than compared to corresponding analyses of 2D dust clusters (see, e.g., Ref. [3]). There, the error in particle positioning is much smaller than in these 3D experiments and thus the Brownian trajectories are more precisely determined.

The spectral power density has its maximum in a stripe increasing from low frequencies at low wave numbers to about 5 Hz at the highest wave numbers. This is very well in the expected frequency range.

Also for these normal modes, we have calculated their respective shear and compressional contribution according to Eq. (8). The result is shown in Fig. 8. It is seen that low mode numbers (which are found at low frequencies) are

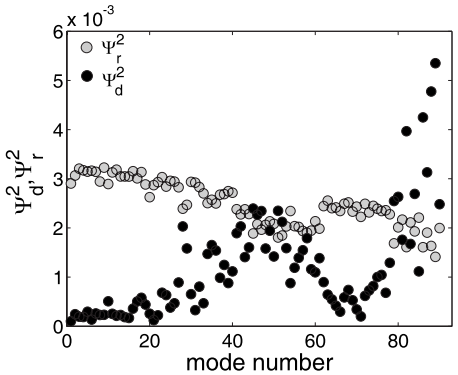

FIG. 8. Shear (Ψ_r^2) and compressional (Ψ_d^2) contribution of the normal modes of the $N=31$ Yukawa ball.

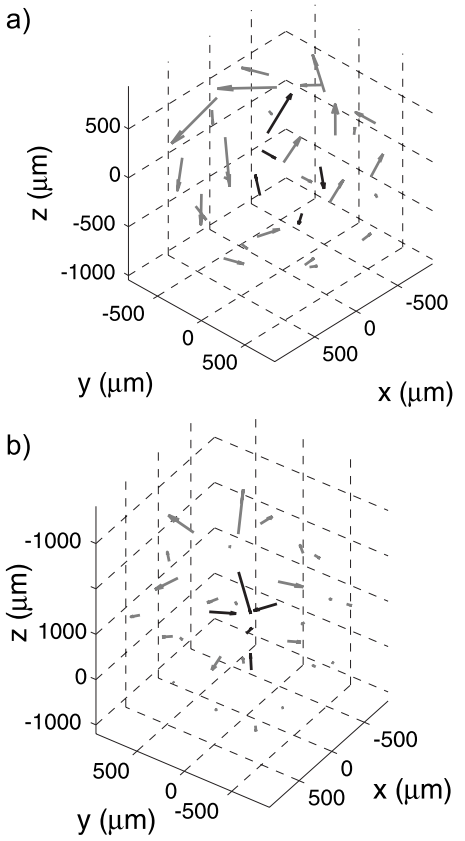

FIG. 9. (a) 3D mode pattern of the intershell rotation mode (normal mode No. 7) and (b) the mode with highest frequency (mode No. 90).

dominated by the shear contribution whereas the high-frequency modes are mainly compressional. This finding is very similar to that of 2D dust clusters.

As for the SVD modes, we also like to exemplify the dynamics with two selected modes (see Fig. 9). First, also in the normal modes an intershell rotation is found, Fig. 9(a). The differential rotation of inner and outer shell is easily recognized. This mode is mode No. 7 and consequently has a very low frequency. That means that the Yukawa ball is easily deformed along this mode pattern. In contrast, mode No. 90 is the mode of highest frequency (the three center-of-mass modes are not considered, here). Here, a quite well-defined pattern is observed: The particles of the inner shell move coherently towards the center whereas the particles of the outer shell are in opposite phase moving outwards. Thus, this mode shows a dominant compressional and rarefractional behavior that leads to the high frequency of this mode.

Returning to the power spectral density in Fig. 7, information of the confinement and the charge can be derived from the mode frequencies. The mode frequencies obtained as the eigenvalues of the dynamical matrix equation (2) effectively depend only on the strength of the confinement ω_0. By fitting the expected eigenfrequencies to the observed spectral power density a nice agreement is obtained and the confinement frequency is readily obtained with $\omega_0/(2\pi) = 2.3$ Hz. The fitted frequencies are shown as circles in Fig. 7. From the physical dimensions of the Yukawa ball and ω_0

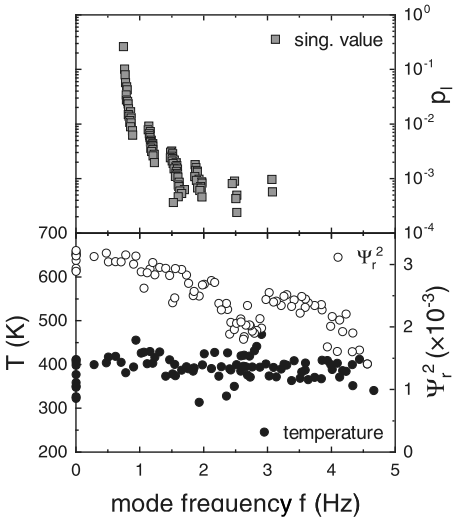

FIG. 10. Mode temperature and shear contribution Ψ_r^2 determined from the normal mode analysis and signal energy values p_ℓ determined from SVD as a function of the mode frequency.

the dust charge is determined as $Z \approx 900$ for our 3.47 μm particles which is similar to the values obtained from structural considerations (there, $Z=1500-2000$ under slightly different discharge conditions) [15,16,18]. The screening strength chosen for the fitting procedure (in experiments, typically, $\kappa=0-3$) does not significantly influence the derived charge values. [Since the average experimental particle positions and trajectories are used to calculate the eigenfrequencies the particles are not exactly in a minimum energy configuration as assumed by the energy equation (1). As a consequence, the eigenfrequencies that describe a harmonic expansion around the equilibrium positions are found as small imaginary values for the first 10 modes. In Fig. 7 these eigenfrequencies are set to zero.]

Finally, it is seen that the equipartition of energy among the normal modes holds for our Yukawa balls system. Figure 10 shows the mode temperatures calculated from Eq. (5) for all the modes as a function of the respective mode frequency. The mode temperature is nearly the same for all of the modes and is found to be 392 K (with an rms deviation of 28 K). Similar temperatures have been obtained for 2D dust clusters [3]. The slight additional heating above room temperature is assumed to be due to stochastic charge and electric field fluctuations [23].

D. Discussion

From the SVD and normal mode analysis a consistent picture of the dynamics of the Yukawa balls is obtained. The most dominating modes (those with the highest contribution to the trajectories, i.e., signal energy) are modes with a high shear contribution, such as rotations, large-scale vortices or intershell rotations. Exactly these modes have the lowest eigenfrequencies. Thus, the Yukawa ball is most easily driven along these low-frequency modes. This means that the dust system is most unstable with respect to these modes.

The preference for these shear modes is, on the one hand, the coupling of the particles to the neutral gas background

since the experiments are performed at relatively high gas pressure. Since the mean free path of the gas molecules still is of the order of or larger than the interparticle distance in the Yukawa ball the neutral gas will preferably drive large scale dynamical processes.

On the other hand, due to the use of relatively small particles with about 900 elementary charges, the Yukawa ball is close to melting. The Coulomb coupling parameter $\Gamma = Z^2e^2/(4\pi\epsilon_0 bkT)$ is then estimated to be of the order of 100 which is close to the solid-liquid transition of extended systems [24]. Finite systems show a melting transition at even higher values of Γ [14] than extended systems. Melting in finite systems first occurs along the most unstable shearlike modes "angular melting" before transitions between shells are observed "radial melting" [25,26].

This is substantiated in Fig. 10 where the rotor and the mode temperature (obtained from the normal modes) are compiled together with the signal energy (obtained from SVD) as a function of mode frequency. The modes with lowest frequencies, that are responsible for melting, are preferably shear modes. Since all the modes contain nearly the same thermal energy the low-frequency modes experience larger mode oscillation amplitudes. Larger excursion amplitudes, in turn, are reflected by higher signal energies. This suggests that the Yukawa ball indeed is close to angular melting. It should be noted, that in long-run experiments very slow transitions of particles between different shells of the Yukawa ball have been observed [16] supporting that the Yukawa ball is close to melting.

Concluding, both the neutral gas coupling and the proximity to melting will certainly enhance the observed features of the preference of shearlike modes in Yukawa balls.

IV. SUMMARY

The dynamical properties of Yukawa balls have been analyzed. From the thermal Brownian motion of the particles in the Yukawa ball around their equilibrium positions the dynamic modes have been derived using singular value decomposition and normal mode analysis.

A prerequisite was that the 3D trajectories of all particles have been reconstructed through an entire sequence of about 1000 frames with a reconstruction error decisively smaller than the thermal motion.

The SVD analysis has revealed that the observed motion of the particles is predominantly from large-scale shear modes such as vortices or intershell rotation. From the normal mode analysis these modes are found to have the lowest frequencies driving the Yukawa ball unstable along these modes.

The preference of these large-scale shear modes are related to the coupling with the neutral gas and the fact that the system is close to melting.

With this the thermodynamic properties of the Yukawa balls can now be addressed using mode analysis techniques.

[1] F. Baletto and R. Ferrando, Rev. Mod. Phys. **77**, 371 (2005).
[2] W.-T. Juan, Z.-H. Huang, J.-W. Hsu, Y.-J. Lai, and L. I, Phys. Rev. E **58**, R6947 (1998).
[3] A. Melzer, Phys. Rev. E **67**, 016411 (2003).
[4] O. Arp, D. Block, A. Piel, and A. Melzer, Phys. Rev. Lett. **93**, 165004 (2004).
[5] T. Antonova, B. M. Annaratone, D. D. Goldbeck, V. Yaroshenko, H. M. Thomas, and G. E. Morfill, Phys. Rev. Lett. **96**, 115001 (2006).
[6] M. Bonitz, D. Block, O. Arp, V. Golubnychiy, H. Baumgartner, P. Ludwig, A. Piel, and A. Filinov, Phys. Rev. Lett. **96**, 075001 (2006).
[7] H. Haberland, T. Hippler, J. Donges, O. Kostko, M. Schmidt, and B. von Issendorff, Phys. Rev. Lett. **94**, 035701 (2005).
[8] M. Klindworth, A. Melzer, A. Piel, and V. A. Schweigert, Phys. Rev. B **61**, 8404 (2000).
[9] A. Melzer, M. Klindworth, and A. Piel, Phys. Rev. Lett. **87**, 115002 (2001).
[10] Y. Ivanov and A. Melzer, Phys. Plasmas **12**, 072110 (2005).
[11] V. M. Bedanov and F. M. Peeters, Phys. Rev. B **49**, 2667 (1994).
[12] V. A. Schweigert and F. M. Peeters, Phys. Rev. B **51**, 7700 (1995).
[13] Y.-J. Lai and L. I, Phys. Rev. E **60**, 4743 (1999).
[14] J. P. Schiffer, Phys. Rev. Lett. **88**, 205003 (2002).
[15] D. Block, S. Käding, A. Melzer, A. Piel, H. Baumgartner, and M. Bonitz, Phys. Plasmas **15**, 040701 (2008).
[16] S. Käding, D. Block, A. Melzer, A. Piel, H. Kählert, P. Ludwig, and M. Bonitz, Phys. Plasmas **15**, 073710 (2008).
[17] T. Antonova, B. M. Annaratone, H. M. Thomas, and G. E. Morfill, New J. Phys. **10**, 043028 (2008).
[18] O. Arp, D. Block, M. Klindworth, and A. Piel, Phys. Plasmas **12**, 122102 (2005).
[19] E. Anderson *et al.*, *LAPACK User's Guide*, 3rd ed. (Society for Industrial and Applied Mathematics, Philadelphia, 1999).
[20] G. H. Golub and C. F. V. Loan, *Matrix Computations (Johns Hopkins Studies in Mathematical Sciences)* (Johns Hopkins University Press, Baltimore, 1996).
[21] T. Trottenberg, D. Block, and A. Piel, Phys. Plasmas **13**, 042105 (2006).
[22] H. Baumgartner, V. Golobnychiy, D. Asmus, P. Ludwig, and M. Bonitz, New J. Phys. (to be published).
[23] R. A. Quinn and J. Goree, Phys. Rev. E **61**, 3033 (2000).
[24] S. Hamaguchi, R. T. Farouki, and D. H. E. Dubin, Phys. Rev. E **56**, 4671 (1997).
[25] M. Kong, B. Partoens, and F. M. Peeters, Phys. Rev. E **67**, 021608 (2003).
[26] S. Apolinario, B. Partoens, and F. Peters, New J. Phys. **9**, 283 (2007).